*Emerging Topics in Life Sciences* (2018) **2** 81–92
https://doi.org/10.1042/ETLS20170086

Review Article

# Cryo-soft X-ray tomography: using soft X-rays to explore the ultrastructure of whole cells

**Maria Harkiolaki, Michele C. Darrow, Matthew C. Spink, Ewelina Kosior, Kyle Dent and Elizabeth Duke**

Diamond Light Source, Harwell Science and Innovation Campus, Didcot, Oxfordshire, U.K.

**Correspondence:** Maria Harkiolaki (maria.harkiolaki@diamond.ac.uk)

Cryo-soft X-ray tomography is an imaging technique that addresses the need for mesoscale imaging of cellular ultrastructure of relatively thick samples without the need for staining or chemical modification. It allows the imaging of cellular ultrastructure to a resolution of 25–40 nm and can be used in correlation with other imaging modalities, such as electron tomography and fluorescence microscopy, to further enhance the information content derived from biological samples. An overview of the technique, discussion of sample suitability and information about sample preparation, data collection and data analysis is presented here. Recent developments and future outlook are also discussed.

## Introduction

The imaging field in the life sciences has flourished in the past few decades and currently delivers 3D cellular imaging of impressive content at a range of resolutions (Figure 1). Electron tomography sets the bar in cellular imaging resolution [1,2], providing highly detailed views of thin biological samples, while fluorescence imaging, in conjunction with endogenous fluorescent labels, reveals intricate molecular interactions within whole cells [3,4], but at a lower resolution. Addressing this resolution gap, and as a direct result of a growing appetite for ever more diverse, cutting-edge imaging applications, cryo-soft X-ray tomography (cryo-SXT) has developed into a key player in the field. Cryo-SXT is a 3D imaging method for the visualisation of cellular ultrastructure at an intermediate resolution [5] and specifically addresses the need for detailed, 3D information on cellular features in thick specimens, such as whole cells, with little or no chemical or mechanical modification (Figure 2). It allows the observation of biological events on a range of scales, with imaging of details as fine as the internal structure of larger viruses and bacteria to the ultrastructure of yeast, protozoa and mammalian cells (Table 1A) and their associated components such as the nucleus, endoplasmic reticulum, mitochondria, parts of the cytoskeleton and more [47]. Many key cellular processes have been investigated to date with cryo-SXT such as chromatin rearrangement, virus–host interactions, cell motility, parasite life cycle, and lymphocyte activation and function (Table 1B).

Historically, the possibility of using X-rays to explore the ultrastructure of cells had been considered since the very discovery of X-rays by Röntgen in 1895 [51]. However, progress was hindered by the lack of X-ray sources and suitable optics until the 1970s when Fresnel zone plates first became available [52,53]. The following two decades saw intense effort concentrated on the development of X-ray microscopy for cellular imaging made possible by the availability of synchrotron sources, improved zone plates, specialised sample chambers and high-resolution direct detection cameras. By the 1990s, a thriving community of researchers was working hard to make use of the full capacity of the technique [54]. Pioneering in the area was the team of the Göttingen beamline at the Bessy storage ring in Berlin that went on to demonstrate the first use of X-ray microscopy on cryogenically preserved cells [43] (a sample preparation method previously validated in the field of electron microscopy [55,56]), thus heralding the dawn of cryogenic X-ray microscopy for biological specimens. Until this pivotal point, radiation damage from exposure to X-rays was a serious limitation in imaging biological samples [57]. Cryo-preservation significantly increased the radiation dose a sample could withstand

Received: 26 November 2017
Revised: 31 January 2018
Accepted: 2 February 2018

Version of Record published:
29 March 2018

© 2018 The Author(s). This is an open access article published by Portland Press Limited on behalf of the Biochemical Society and the Royal Society of Biology and distributed under the Creative Commons Attribution License 4.0 (CC BY).

Emerging Topics in Life Sciences (2018) **2** 81–92
https://doi.org/10.1042/ETLS20170086

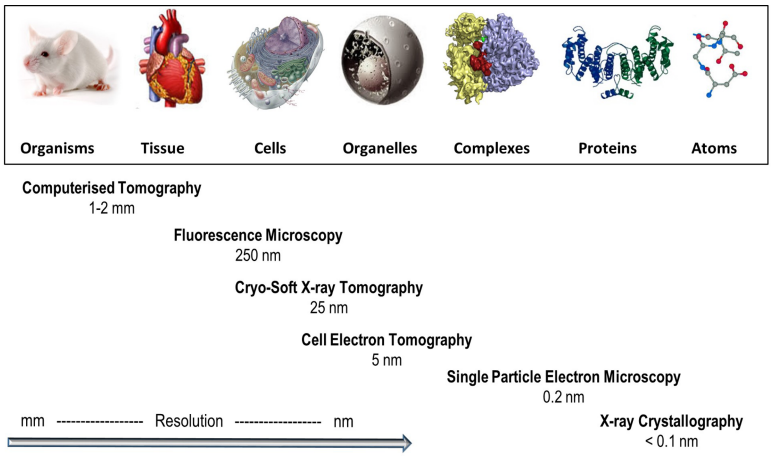



**Figure 1. Biological imaging in context.**

Representative techniques developed for the investigation of structure in biological systems at different scales, in order of resolution attainable.

prior to large-scale damage [58–60] and therefore allowed longer exposures and serial imaging, leading to the current implementations of cryo-SXT. Efforts since have led to the evolution of cryo-SXT into a user-friendly and accessible method [6,44,61] generating an ever-increasing volume of data (Table 1A,B). Further development of its capabilities and algorithm development for data processing, evaluation and analysis [10,19,62,63], and correlation with other imaging modalities [30,40,64,65] are currently areas of intense interest.

Presently, cryo-SXT is available at many synchrotron beamlines across the globe [6,44,61] (Table 2) delivering high-contrast, cellular imaging up to a resolution of 25 nm [66]. For example, at the UK synchrotron, Diamond Light Source, the cryo-SXT beamline B24 (Figure 3 and Table 3) uses X-rays from a bending magnet on the synchrotron ring, which are passed to focusing and dispersive optics before reaching the microscope (UltraXRM-S220c Zeiss) vessel. There, they are delivered via a capillary condenser to the sample plane [67] and focused on the imaging plane of a camera with a Fresnel zone plate. Table-top set-ups using soft X-rays

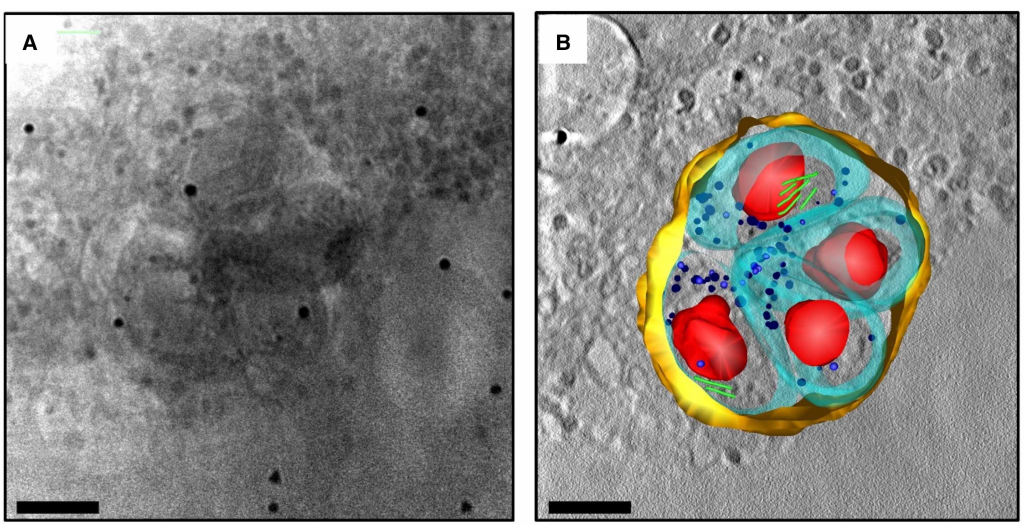



**Figure 2. An example of typical cryo-SXT data.**

(**A**) A cryo-STX projection image of a *Toxoplasma gondii* containing vacuole within a human fibroblast cell. The reconstructed volume (**B**) shows the parasitophorous vacuole in yellow containing four parasites (plasma membranes in cyan and rhoptries in green) with their respective nuclei in red. The bars are 2.5 μm. Data collected at B24. Image courtesy of Katja Ota and Hellen Saibil (Birkberk College London, U.K.).



© 2018 The Author(s). This is an open access article published by Portland Press Limited on behalf of the Biochemical Society and the Royal Society of Biology and distributed under the Creative Commons Attribution License 4.0 (CC BY).

**Table 1A Representative cells and organisms that have been examined by cryo-SXT**

| | |
|---|---|
| Bacteria | *Leptothrix orchacea* [6], *Escherichia coli* [7,8], *Mycobacterium smegmatis* [7], *Salmonella enterica* [9] |
| Yeast | *Saccharomyces cerevisiae* [10–12], *Saccharomyces pombe* [7,11–13], *Candida albicans* [7,11,12] |
| Algae | *Chlamydomonas reinhardtii* [14], *Scenedesmus*[15] |
| Plankton | *Emiliania huxleyi* [16] |
| Protozoa | *Plasmodium falcitatum* [17,18], *Trypanosoma brucei* [19], *Toxoplasma gondii* (Figure 3) |
| Viruses | Vaccinia [20,21], Herpes Simplex Virus 1 [22,23], Hepatitis C [24] |
| Primary cells | Erythrocytes [25,26], lymphocytes [9,12,22,27], olfactory sensory neurones [28,29] |
| Immortalised lines | EFN-R [30], HEK293 [31,32], G361 [33], RK13 [34], Cos7 [35], MCF-7 [36,37], Huh7 [38], RBL-2H3 [39], RAW264.7 [40], T-cell CEM [41], HT1080 [5], HT29 [15], J774 [42], PtK2 [20,43,44], 3T3 [42,45], DF1 [20], PC12 [19], mouse adenocarcinoma [25,46] |

**Table 1 B Representative biological processes studied with cryo-SXT to date**

| | |
|---|---|
| Virus–host interactions (membrane remodelling) [48] | Mitochondrial fission [35] |
| Chromatin reorganisation [22,23,28] | Phenotypic switching in yeast [45] |
| Assembly of viral factories [20] | Cholesterol crystal formation in macrophages [40] |
| *Plasmodium* haeme detoxification [17] and egress [49] | ER restructuring in HCV infection [24] |
| Clathrin-dependent cell motility in lymphocytes [41] | Calcium concentrates in algae [16] |
| Differentiation-induced chromatin distribution [28] | Nanoparticle adsorption by cells [42,50] |
| Erythrocyte physiology in disease [26] | Bacterial activation of T lymphocytes [9] |
| Degranulation in mast cells [39] | |

generated by a plasma source have also been described [68], but suffer from lower flux when compared with synchrotron sources, resulting in much longer acquisition times. Access to cryo-SXT is possible through many international synchrotron facilities (Table 1), where new users can work with technique experts to ascertain project feasibility and receive advice on experiment design.

# Theory of cryo-SXT

In cryo-SXT, 2D images are formed when an X-ray beam travels through an object and is differentially attenuated or scattered by structures in its path [54]. When X-rays emerge from the sample, they effectively carry the likeness of that object, which they deliver to a camera, resulting in a 2D projection of the 3D sample. Single 2D projections, however, provide only limited volumetric information since they carry no information about the relative depth of various features. To generate a 3D volume of the contents of a cell, 2D projections are recorded at discrete angular increments about a sagittal rotation axis to create a tilt series of images that present structural features at different relative orientations [1]. Tilt series are then reconstructed into

**Table 2 Synchrotron-based soft X-ray tomography beamlines**

| | Beamline | Facility | Location |
|---|---|---|---|
| Operational | U41-TXM | Bessy II | Berlin, Germany |
| | XM2 | Advanced Light Source (ALS) | Berkeley, California, U.S.A. |
| | Mistral | ALBA | Barcelona, Spain |
| | B24 | Diamond Light Source (DLS) | Didcot, U.K. |
| Under construction | 24A | Taiwan Photon Source | Hsinchu, Taiwan |
| | — | Shanghai Synchrotron Radiation Facility | Shanghai, China |
| | 10ID1 | Canadian Light Source | Saskatoon, Canada |

© 2018 The Author(s). This is an open access article published by Portland Press Limited on behalf of the Biochemical Society and the Royal Society of Biology and distributed under the Creative Commons Attribution License 4.0 (CC BY).

Emerging Topics in Life Sciences (2018) **2** 81–92
https://doi.org/10.1042/ETLS20170086

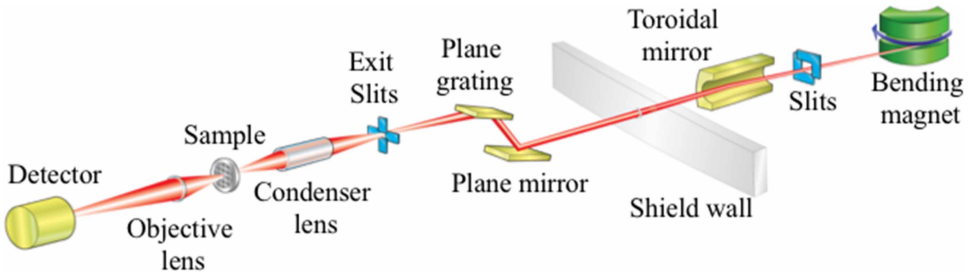



**Figure 3. A schematic of beamline B24 at the Diamond Light Source synchrotron.**
X-rays are produced at a bending magnet, focused by a toroidal mirror and conditioned with a plane grating monochromator resulting in a secondary source at the exit slits. X-rays from his source are focused by capillary condenser lens and the resulting projections are directed via a zone plate objective to the detector.

tomograms, via either Fourier or real-space methods, to produce a volumetric representation of cellular contents [69]. These tomograms are effectively the cellular equivalent of the common computed tomography (CT) scans routinely performed in medical settings.

Cryo-SXT can deliver images either by absorption contrast at defined spectral areas [54] or by phase contrast through a reference wave front at higher X-ray energies [70]. Absorption contrast is the current standard in the field and it takes advantage of the absorption characteristics of biological matter at the 'water window' [the spectral region defined by the X-ray absorption edges of carbon (284 eV) and oxygen (543 eV)] [71]. X-rays within this region are absorbed an order of magnitude more by carbon- and nitrogen-rich biological structures when compared with the oxygen-rich medium that surrounds them. This relative difference generates contrast in the projections of a cellular area.

There are many inherent benefits in cryo-soft X-ray imaging. Given the natural absorption contrast resulting from carbon-rich biological structures, there is no need for additional sample staining. Moreover, the penetration depth of soft X-rays through biological matter is several microns, and as a result, X-rays can effectively travel the width of a single cell without substantial dissipation; cells therefore do not need to be sectioned or milled to

**Table 3 Beamline B24 design specifications**

| |
|---|
| Beamline acceptance: 2 × 2 mrad |
| Beam focusing via a single toroidal mirror delivering 1 : 1 magnification |
| Plain grating monochromator with variable line spacing gratings delivering 200–2600 eV |
| Resolving power >1700 |
| Beam size at sample: 20 μm |
| Photon flux at sample: $10^8$ photons/$\mu m^2$ |
| End Station: Xradia* UltraXRM-S220c |
| Resolution: 25 and 40 nm (Xradia zone plate optic) |
| Detector: Direct detection CCD (Pixis-XO:1024B, Princeton Instruments) |
| Techniques possible: absorption- and phase-contrast modes |
| **Commissioned operation parameters** |
| Absorption contrast at 500 eV (water window) with a 40 nm zone plate |
| Samples mounted or grown on 3 mm grids, 4× grids loaded at a time |
| Magnification delivered: |
| Data collection strategy: tilt series −70° to +70°, 0.5° steps |
| Data handling: automated backup and reconstruction |
| In-line fluorescence detection capability |

*Xradia is now part of the Carl Zeiss X-ray Microscopy group.



© 2018 The Author(s). This is an open access article published by Portland Press Limited on behalf of the Biochemical Society and the Royal Society of Biology and distributed under the Creative Commons Attribution License 4.0 (CC BY).

suitably thin samples [54]. Finally, due to cryo-preservation, chemical fixation (to minimise sample drift during data collection and confer resistance to radiation damage) is unnecessary [43]. Hence, cryo-SXT can deliver structural information on cellular ultrastructure on whole cells in a near-native state. Correlation with further imaging modalities is another appealing feature of cryo-SXT. The 3D volume displaying the ultrastructure of a cell produced by cryo-SXT can be correlated with 2D and 3D fluorescence microscopy to localise events or features of interest. This allows for the evaluation of molecular function with respect to localisation within a cell. Many studies, to date, have used fluorescence microscopy and cryo-SXT correlative approaches, showcasing the wealth of detailed information that can be acquired in this way [13,24,25,27,30,31,34–36,39,40,45,64].

In summary, cryo-SXT is an imaging modality that can provide ultrastructural information, with a resolution range of 40–25 nm, of a whole, intact cell, without the need for fixation, dehydration or staining to prepare the sample for imaging. It has generally been used to study whole cells; however, imaging tissue preparations and non-biological composites is also possible with cryo-SXT. Using this technique, especially in conjunction with other correlative imaging modalities, questions about the effects of stimuli or treatment, or the process of disease or infection, can be studied.

# Cryo-SXT workflow

Here, we provide an example workflow describing the steps involved in preparing samples for cryo-SXT, followed by acquiring and processing cryo-SXT data (Figure 4).

## Sample preparation

For the purposes of this review, the discussion will focus on experimental parameters that are relevant to beamlines, such as B24, that are designed to use standard or modified electron microscopy grids [44,64]. An alternative set-up is used at the XM2 beamline at the ALS synchrotron where samples in suspension can be loaded into thin-walled glass capillary tubes [61] that serve as sample holders.

Typical cryo-SXT samples are adherent or non-adherent cells; however, the technique can also accommodate the imaging of tissue sections or separated cellular contents. Often, fluorescent markers are endogenously expressed or added to cell culture media. For adherent cell lines, the cells are cultured on 3.05 mm gold transmission electron microscopy (TEM) grids [72]. Prior to cell culture, the grids are coated with a carbon substrate [30,31] to provide a retaining surface for cells and that surface is further treated by either glow discharge or plasma cleaning to increase hydrophilicity. To encourage cell attachment and spreading, the carbon film may also be treated with adherence-promoting agents such as ornithine, poly-D-lysine or laminin [73–75]. Conventional brightfield microscopy can be used to evaluate cell attachment and growth on the grids with the general goal of ∼40% confluency and a good distribution of individual cells. Fluorescence detection techniques, such as confocal microscopy, can be used to document successful endogenous expression of fluorescent markers.

Plunge freezing [76] is currently the method of choice for sample preservation for cryo-SXT, although high-pressure freezing [77] is better suited to thicker samples (>10 μm). In plunge freezing, vitrification is achieved via rapid cooling to temperatures below −170°C by plunging the sample grid into liquid nitrogen-cooled liquid ethane or propane. Prior to this step, gold nanoparticle fiducial markers are added (100–250 nm diameter) for later use during the process of tilt series reconstruction [31] and excess liquid is blotted away reducing the depth of the sample, ideally to just thicker than a single layer of cells. After plunge freezing, samples can be stored at liquid nitrogen temperatures indefinitely.

## Pre-mapping and correlative imaging

Samples should be evaluated for suitability prior to a cryo-SXT experiment, as plunge freezing can be unsuccessful for many reasons. A cryostage-equipped light microscope can be used to examine grids and confirm that cells have retained their gross morphology, and that the grid does not have ice contamination or many large breaks in the support film. Samples can also be pre-mapped in brightfield and fluorescence (Figure 5A,B), as appropriate, and areas of interest can be identified for 3D data collection. If fluorescent markers are present, it is entirely appropriate at this point to examine their distribution with super-resolution fluorescence cryo-microscopy methods before the fluorophores present are compromised by exposure to X-rays. 3D super-resolution imaging techniques, such as cryo-structured illumination microscopy (cryo-SIM) [78] (available on beamline B24 through a collaboration with the advanced bioimaging unit, Micron, at the University of Oxford, UK), are particulary suited to correlation with cryo-SXT as they can provide a stack of relatively high-resolution images (∼200 nm) through the sample, mapping in 3D the intracellular location of fluorophores.

© 2018 The Author(s). This is an open access article published by Portland Press Limited on behalf of the Biochemical Society and the Royal Society of Biology and distributed under the Creative Commons Attribution License 4.0 (CC BY).

Emerging Topics in Life Sciences (2018) **2** 81–92
https://doi.org/10.1042/ETLS20170086

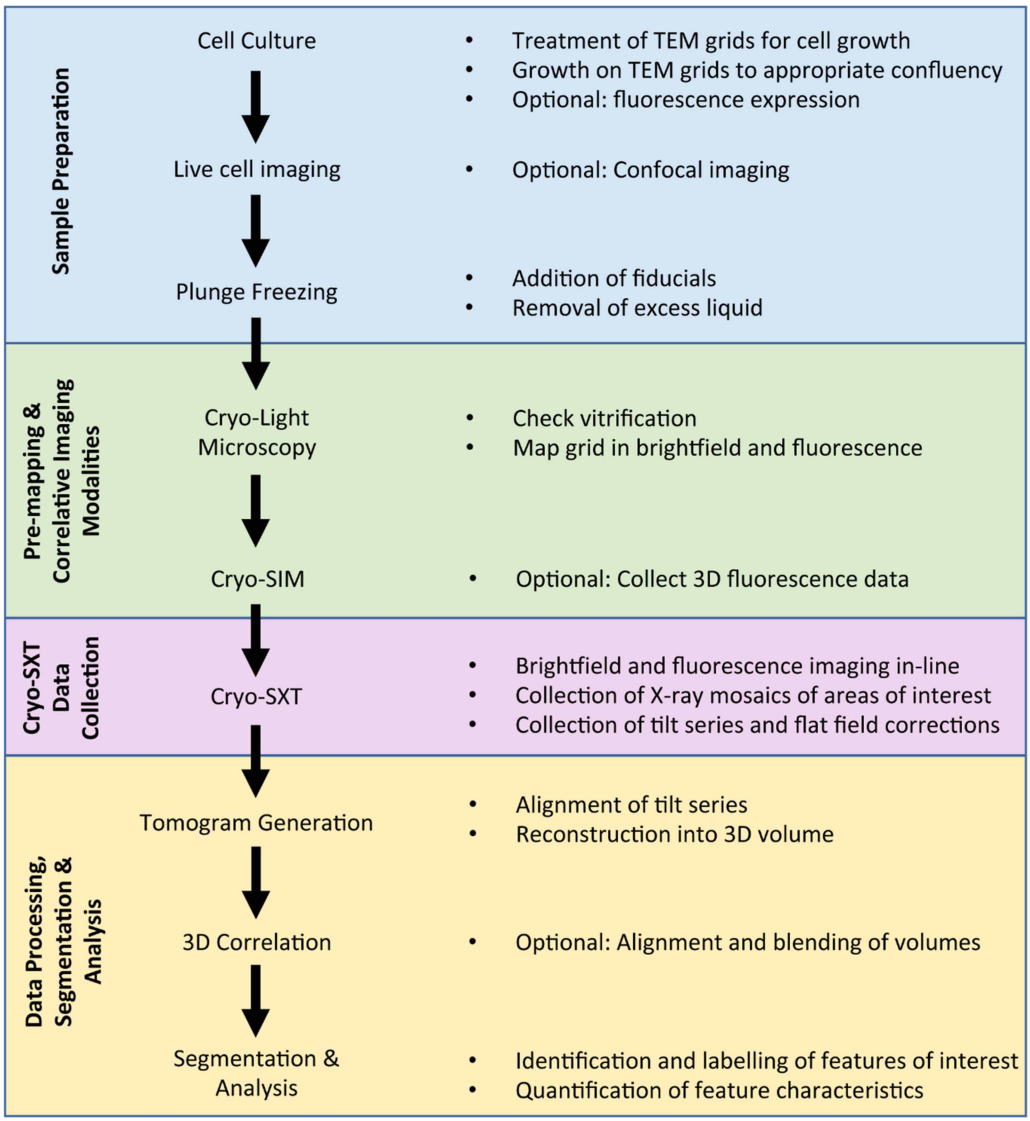



**Figure 4. Cryo-SXT workflow.**

## Cryo-SXT data collection

At beamline B24, sample grids are placed into the X-ray microscope vessel using a transfer chamber that allows the transition from liquid nitrogen storage under atmospheric pressure to cooling via conduction under high vacuum. Grids are placed at the imaging position in close proximity to the microscope optics (during imaging, optics are only few millimetres away) where they can be examined using an in-line conventional light microscope (20× objective at B24) for a final inspection of the sample and the opportunity to locate the exact areas previously mapped at higher resolutions in other imaging modalities. Because the light microscope is in-line, a common set of working co-ordinates can be assigned in order to return to the same area for X-ray imaging (Figures 5C and 6A).

Whole grid squares are examined using low-dose X-ray exposures and collation of adjacent stills into mosaic images (Figures 5D and 6B), which provide overviews of whole cells in the region of interest. Mosaics are needed because the field of view of transmission X-ray microscopes tends to be 20 μm or less and adherent cells are often substantially larger. Specific areas are identified for tilt series acquisition and for each, the maximum rotation prior to obstruction and appropriate angular steps and exposure times are determined. If a single field of view is insufficient for the experiment, adjacent overlapping tilt series can be collected and later



© 2018 The Author(s). This is an open access article published by Portland Press Limited on behalf of the Biochemical Society and the Royal Society of Biology and distributed under the Creative Commons Attribution License 4.0 (CC BY).

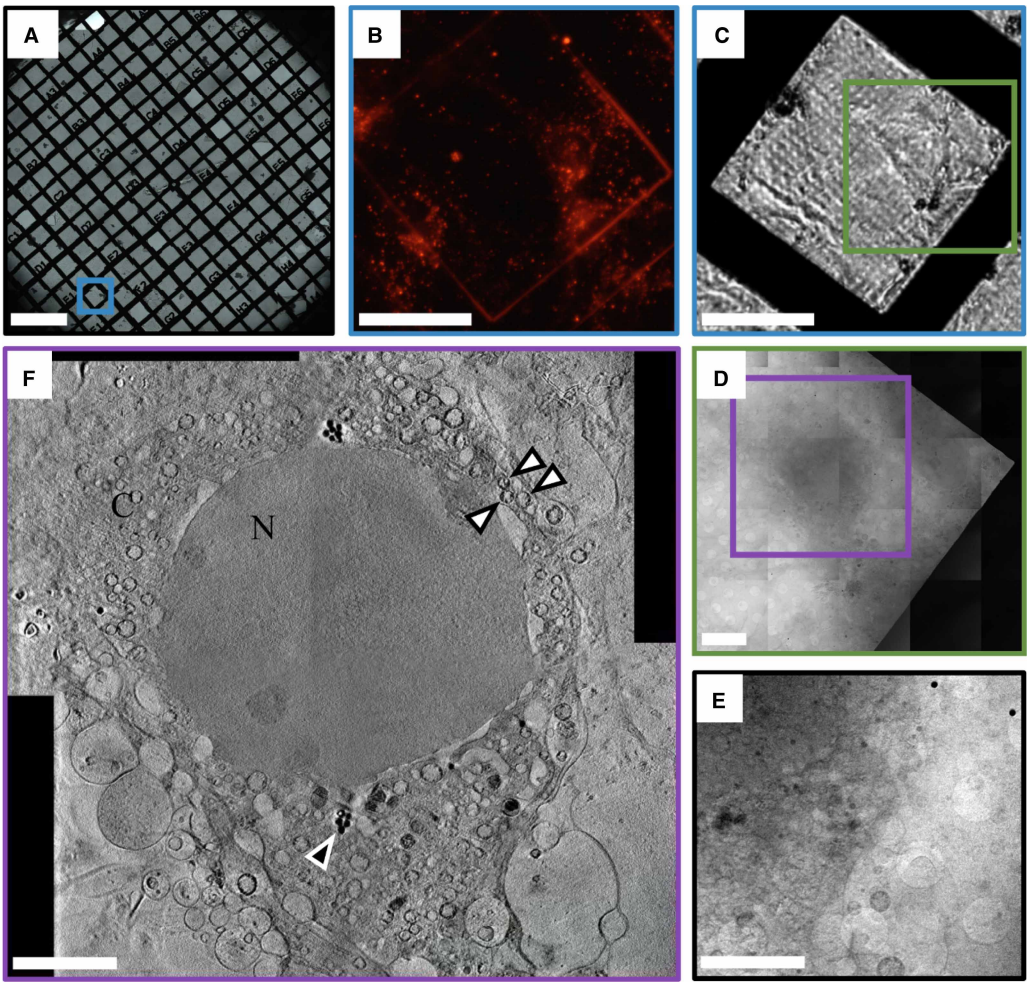



**Figure 5. Typical cryo-STX imaging progression for adherent cells with fluorescence labels.**
(**A**) Brightfield grid overview of cryo-preserved mouse primary neuronal cells on a TEM grid (bar = 500 μm), (**B**) close-up fluorescence and (**C**) brightfield images of the area on **A** marked by a blue square (bar = 50 μm), (**D**) X-ray mosaic of the area marked in **C** (bar = 10 μm), (**E**) single field or view X-ray projection and (**F**) slice through a cumulative tomogram, showing the nucleus (N) and surrounding vesicles in the cytoplasm (C) produced by stitching four tomograms collected in adjacent overlapping areas. Bars for **E** and **F** = 5 μm; black arrow with white outline points to lipid droplets, white arrows with black outline point to mitochondria; Data collected at B24. Image courtesy of Karen Marshall and Louise Serpell at Sussex University, U.K.

computationally merged (Figure 5F). Generally, for a flat TEM grid, tilt series are collected from ±65° with a step size of 0.5° or 1°. Exposure times are dependent on X-ray flux and sample thickness, but are generally in the range of a few seconds per projection. Depending on the parameters chosen, tilt series acquisition generally takes ∼5–20 min in total. Background flat field images are collected regularly to correct for fixed pattern noise present in the beam.

For a flat TEM grid, the maximum rotation possible is limited both by the attenuation of the beam due to increased sample thickness at high tilts and by the physical proximity of the X-ray optics to the grid. This limited rotation tilt series results in 'missing wedge' artefacts, named after the shape of the missing information in Fourier space. The rotation restriction is less problematic when using a modified, flat grid [64] and in the case of a glass capillary tube, a full rotation tilt series can be collected, alleviating the issues created by the missing wedge [6]. However, currently, glass capillary tubes are more suited to imaging cell suspensions, while flat grids can accommodate both cell suspensions and adherent cell preparations. Irrespective of the sample holder, the depth of focus at the sample plane is generally smaller than the total depth of the sample being imaged, leading to some blurring of out-of-focus features and possible loss of resolution during the reconstruction process [15].

© 2018 The Author(s). This is an open access article published by Portland Press Limited on behalf of the Biochemical Society and the Royal Society of Biology and distributed under the Creative Commons Attribution License 4.0 (CC BY).

Emerging Topics in Life Sciences (2018) **2** 81–92
https://doi.org/10.1042/ETLS20170086

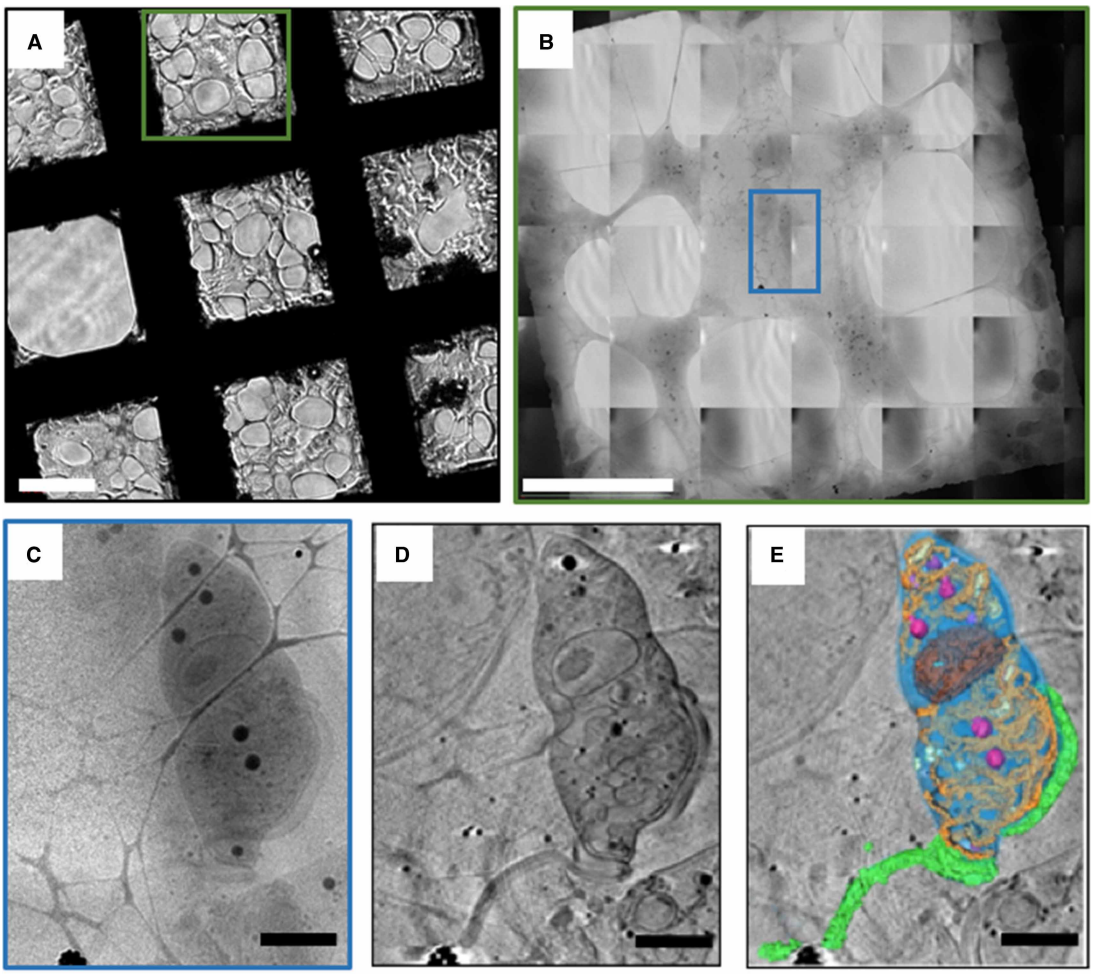



**Figure 6. Typical cryo-STX imaging workflow for smaller samples (*Trypanosome brucei*) with no associated fluorescence.**

(**A**) Brightfield overview of cryo-preserved cells on an area of holey carbon on a TEM grid (bar = 50 μm), (**B**) X-ray mosaic of the area on **A** marked by a green square (bar = 25 μm), (**C**) X-ray projection of the area on **B** marked by a blue square, (**D**) tomogram slice of the same area after reconstruction and (**E**) segmented volumes with delineated cellular ultrastructure (flagellum is green, cell body in blue and organelles in various other colours). Data collected at B24. Image reproduced from Luengo et al. [19].

More sophisticated data collection techniques in cryo-SXT, such as dual tilt series to reduce missing wedge artefacts [80] and focal series data acquisition to circumvent the resolution reduction due to out-of-focus information [15]), are currently pioneered by the Mistral team at ALBA [15] and are likely to be adopted elsewhere soon.

## Data processing, segmentation and analysis

At synchrotrons, as data are collected, they enter a semi- or fully-automated processing pipeline that handles changes in file format, alignment of the tilt series and finally reconstruction into a 3D tomogram. This allows for an initial near real-time data analysis, enabling evaluation of data quality during the data collection process. At B24, for example, tilt series are aligned and reconstructed using the batch reconstruction processes in IMOD [81]. Other in-house alignment and reconstruction software, which is specific to X-ray imaging, is also used elsewhere [63].

The generation of a tomogram from a tilt series depends heavily on the accurate alignment of images within that series. During data collection, individual images can suffer from mechanical misalignments such as rotation drift or motor backlash. If these misalignments are not corrected, they can result in loss of resolution, or the blurring of features, in the 3D tomogram. Fiducial markers, either added during sample preparation or



© 2018 The Author(s). This is an open access article published by Portland Press Limited on behalf of the Biochemical Society and the Royal Society of Biology and distributed under the Creative Commons Attribution License 4.0 (CC BY).

natural fiducials found in the sample, are generally used to align the tilt series. However, it is also possible to align tilt series using patch-based cross-correlation algorithms [79]. In any case, the features of the fiducials, or within the patches, must be high contrast and unique so that their movement can be accurately tracked.

Generally speaking, two main reconstruction algorithms are used in the field of cryo-SXT: weighted back projection (WBP) [82] and simultaneous iterative reconstruction technique (SIRT) [83]. WBP is a Fourier space reconstruction method which can accentuate high-resolution noise, while SIRT is performed in real space, and depending on the number of iterations chosen, can filter high-resolution noise from the resulting tomogram.

While many subcellular organelles can be identified in cryo-SXT tomograms, segmentation is necessary to both meaningfully visualise and analyse this data (Figure 5). Segmentation is the process of delineating and classifying objects or areas of interest throughout the 3D volume. This process can be entirely manual, with a person outlining the boundaries of cellular structures of interest on each slice through the 3D volume [81,84]; or segmentation algorithms can be used to decrease the time and manual input required [19,85–87]. Manual segmentation can be, by far, the most time-consuming step in a cryo-SXT experiment and it is generally regarded as somewhat objective and variable [88]. Recent advances in data representation and segmentation have been introduced at Diamond Light Source through the SuRVoS Workbench, which uses minimal manual training inputs to assign voxels in the volume to user-defined classes [19,89]. Once cellular features have been segmented and classified, further analysis of size, shape and localisation within the context of a whole cell can lead to biological understanding.

Data processing and analysis in the cryo-SXT field is currently in its formative years. While many approaches and software packages can be borrowed and adapted from other fields, ongoing efforts are underway to provide purpose-built software packages specific to the needs of the cryo-SXT community.

## Conclusion and future direction

Currently, cryo-SXT offers an excellent way to visualise the ultrastructure of cells, in order to delineate organelle architecture, membrane organisation and interactions within the cell. In addition, the use of cryo-SXT as a correlative imaging technique can provide large-scale cellular context for data collected via electron tomography or fluorescence microscopy.

Cryo-SXT is still an emerging technique for the life sciences, with a growing user community that will inevitably direct its development and nurture it to maturity. Technical implementation, sample protocols and related applications are widely documented, although the technique does, by and large, remain within the realm of large infrastructures such as synchrotrons. Access through synchrotron sources, however, is available to a great number of researchers across the world and as more cryo-SXT beamlines emerge from commissioning phases, better coverage is projected.

In the future, it is expected that cryo-SXT will deliver better contrast at higher resolutions; data collection, processing and segmentation pipelines will improve, ideally to the point of full automation; associated developments in correlative imaging will ease the current physical and software difficulties in transitioning from one technique to another and cryo-SXT will be established as a robust partner in interdisciplinary approaches.

## Summary

- Cryo-SXT offers near-native imaging of whole cells.
- The method uses the natural absorption of soft X-rays by biological matter to produce projection images of cells.
- Cryo-SXT data can be correlated to fluorescence microscopy and electron microscopy/tomography data.
- Access to the technique is provided primarily via synchrotron facilities.
- Sample preparation methods are well defined and documented.
- Cryo-SXT data handling and analysis protocols are under development.

© 2018 The Author(s). This is an open access article published by Portland Press Limited on behalf of the Biochemical Society and the Royal Society of Biology and distributed under the Creative Commons Attribution License 4.0 (CC BY).

Emerging Topics in Life Sciences (2018) **2** 81–92
https://doi.org/10.1042/ETLS20170086

## Abbreviations

cryo-SXT, Cryo-soft X-ray tomography; SIRT, simultaneous iterative reconstruction technique; TEM, transmission electron microscopy; WBP, weighted back projection.

## Acknowledgements

The authors thank D.I. Stuart, M. Walsh and B. Kaulich at Diamond Light Source for critical reading of the manuscript and helpful suggestions.

## Competing Interests

The Authors declare that there are no competing interests with the manuscript.

## References

1 Diebolder, C.A., Koster, A.J. and Koning, R.I. (2012) Pushing the resolution limits in cryo electron tomography of biological structures. *J. Microsc.* **248**, 1–5 https://doi.org/10.1111/j.1365-2818.2012.03627.x
2 Irobalieva, R.N., Martins, B. and Medalia, O. (2016) Cellular structural biology as revealed by cryo-electron tomography. *J. Cell Sci.* **129**, 469–476 https://doi.org/10.1242/jcs.171967
3 Pawley, J.B. (2006) *Handbook of Biological Confocal Microscopy*. Springer; 985 p
4 Wessels, J.T., Yamauchi, K., Hoffman, R.M. and Wouters, F.S. (2010) Advances in cellular, subcellular, and nanoscale imaging in vitro and in vivo. *Cytometry A* **77**, 667–676 https://doi.org/10.1002/cyto.a.20931
5 Ekman, A.A., Chen, J.-H., Guo, J., McDermott, G., Le Gros, M.A. and Larabell, C.A. (2017) Mesoscale imaging with cryo-light and X-rays: larger than molecular machines, smaller than a cell. *Biol. Cell* **109**, 24–38 https://doi.org/10.1111/boc.201600044
6 Weiß, D., Schneider, G., Niemann, B., Guttmann, P., Rudolph, D. and Schmahl, G. (2000) Computed tomography of cryogenic biological specimens based on X-ray microscopic images. *Ultramicroscopy* **84**, 185–197 https://doi.org/10.1016/S0304-3991(00)00034-6
7 McDermott, G., Fox, D.M., Epperly, L., Wetzler, M., Barron, A.E., Le Gros, M.A. et al. (2012) Visualizing and quantifying cell phenotype using soft X-ray tomography. *BioEssays* **34**, 320–327 https://doi.org/10.1002/bies.201100125
8 Le Gros, M.A., McDermott, G., Uchida, M., Knoechel, C.G. and Larabell, C.A. (2009) High-aperture cryogenic light microscopy. *J. Microsc.* **235**, 1–8 https://doi.org/10.1111/j.1365-2818.2009.03184.x
9 Cruz-Adalia, A., Ramirez-Santiago, G., Calabia-Linares, C., Torres-Torresano, M., Feo, L., Galán-Díez, M. et al. (2014) T cells kill bacteria captured by transinfection from dendritic cells and confer protection in mice. *Cell Host Microbe* **15**, 611–622 https://doi.org/10.1016/j.chom.2014.04.006
10 Parkinson, D.Y., Knoechel, C., Yang, C., Larabell, C.A. and Le Gros, M.A. (2012) Automatic alignment and reconstruction of images for soft X-ray tomography. *J. Struct. Biol.* **177**, 259–266 https://doi.org/10.1016/j.jsb.2011.11.027
11 Uchida, M., Sun, Y., McDermott, G., Knoechel, C., Le Gros, M.A., Parkinson, D. et al. (2011) Quantitative analysis of yeast internal architecture using soft X-ray tomography. *Yeast* **28**, 227–236 https://doi.org/10.1002/yea.1834
12 Larabell, C.A. and Nugent, K.A. (2010) Imaging cellular architecture with X-rays. *Curr. Opin. Struct. Biol.* **20**, 623–631 https://doi.org/10.1016/j.sbi.2010.08.008
13 Smith, E.A., Cinquin, B.P., Do, M., McDermott, G., Le Gros, M.A. and Larabell, C.A. (2014) Correlative cryogenic tomography of cells using light and soft X-rays. *Ultramicroscopy* **143**, 33–40 https://doi.org/10.1016/j.ultramic.2013.10.013
14 Hummel, E., Guttmann, P., Werner, S., Tarek, B., Schneider, G., Kunz, M. et al. (2012) 3D Ultrastructural organization of whole *Chlamydomonas reinhardtii* cells studied by nanoscale soft X-ray tomography. *PLoS ONE* **7**, e53293 https://doi.org/10.1371/journal.pone.0053293
15 Otón, J., Pereiro, E., Conesa, J.J., Chichón, F.J., Luque, D., Rodríguez, J.M. et al. (2017) XTEND: extending the depth of field in cryo soft X-ray tomography. *Sci. Rep.* **7**, 45808 https://doi.org/10.1038/srep45808
16 Sviben, S., Gal, A., Hood, M.A., Bertinetti, L., Politi, Y., Bennet, M. et al. (2016) A vacuole-like compartment concentrates a disordered calcium phase in a key coccolithophorid alga. *Nat. Commun.* **7**, 11228 https://doi.org/10.1038/ncomms11228
17 Kapishnikov, S., Weiner, A., Shimoni, E., Guttmann, P., Schneider, G., Dahan-Pasternak, N. et al. (2012) Oriented nucleation of hemozoin at the digestive vacuole membrane in *Plasmodium falciparum*. *Proc. Natl Acad. Sci. U.S.A.* **109**, 11188–11193 https://doi.org/10.1073/pnas.1118120109
18 Kapishnikov, S., Leiserowitz, L., Yang, Y., Cloetens, P., Pereiro, E., Awamu Ndonglack, F. et al. (2017) Biochemistry of malaria parasite infected red blood cells by X-ray microscopy. *Sci. Rep.* **7**, 802 https://doi.org/10.1038/s41598-017-00921-2
19 Luengo, I., Darrow, M.C., Spink, M.C., Sun, Y., Dai, W., He, C.Y. et al. (2017) SuRVoS: Super-Region Volume Segmentation workbench. *J. Struct. Biol.* **198**, 43–53 https://doi.org/10.1016/j.jsb.2017.02.007
20 Chichón, F.J., Rodríguez, M.J., Pereiro, E., Chiappi, M., Perdiguero, B., Guttmann, P. et al. (2012) Cryo X-ray nano-tomography of vaccinia virus infected cells. *J. Struct. Biol.* **177**, 202–211 https://doi.org/10.1016/j.jsb.2011.12.001
21 Carrascosa, J.L., Chichón, F.J., Pereiro, E., Rodríguez, M.J., Fernández, J.J., Esteban, M. et al. (2009) Cryo-X-ray tomography of vaccinia virus membranes and inner compartments. *J. Struct. Biol.* **168**, 234–239 https://doi.org/10.1016/j.jsb.2009.07.009
22 Myllys, M., Ruokolainen, V., Aho, V., Smith, E.A., Hakanen, S., Peri, P. et al. (2016) Herpes simplex virus 1 induces egress channels through marginalized host chromatin. *Sci. Rep.* **6**, 28844 https://doi.org/10.1038/srep28844
23 Aho, V., Myllys, M., Ruokolainen, V., Hakanen, S., Mäntylä, E., Virtanen, J. et al. (2017) Chromatin organization regulates viral egress dynamics. *Sci. Rep.* **7**, 3692 https://doi.org/10.1038/s41598-017-03630-y
24 Pérez-Berná, A.J., Rodríguez, M.J., Chichón, F.J., Friesland, M.F., Sorrentino, A., Carrascosa, J.L. et al. (2016) Structural changes in cells imaged by soft X-ray cryo-tomography during hepatitis C virus infection. *ACS Nano* **10**, 6597–6611 https://doi.org/10.1021/acsnano.6b01374
25 McDermott, G., Le Gros, M.A. and Larabell, C.A. (2012) Visualizing cell architecture and molecular location using soft X-ray tomography and correlated cryo-light microscopy. *Annu. Rev. Phys. Chem.* **63**, 225–239 https://doi.org/10.1146/annurev-physchem-032511-143818



© 2018 The Author(s). This is an open access article published by Portland Press Limited on behalf of the Biochemical Society and the Royal Society of Biology and distributed under the Creative Commons Attribution License 4.0 (CC BY).

26 Darrow, M.C., Zhang, Y., Cinquin, B.P., Smith, E.A., Boudreau, R., Rochat, R.H. et al. (2016) Visualizing red blood cell sickling and the effects of inhibition of sphingosine kinase 1 using soft X-ray tomography. *J. Cell Sci.* **129**, 3511–3517 https://doi.org/10.1242/jcs.189225
27 Smith, E.A., McDermott, G., Do, M., Leung, K., Panning, B., Le Gros, M.A. et al. (2014) Quantitatively imaging chromosomes by correlated cryo-fluorescence and soft X-ray tomographies. *Biophys. J.* **107**, 1988–1996 https://doi.org/10.1016/j.bpj.2014.09.011
28 Le Gros, M.A., Clowney, E.J., Magklara, A., Yen, A., Markenscoff-Papadimitriou, E., Colquitt, B. et al. (2016) Soft X-ray tomography reveals gradual chromatin compaction and reorganization during neurogenesis in vivo. *Cell Rep.* **17**, 2125–2136 https://doi.org/10.1016/j.celrep.2016.10.060
29 Isaacson, S.A., Larabell, C.A., Le Gros, M.A., McQueen, D.M. and Peskin, C.S. (2013) The influence of spatial variation in chromatin density determined by X-ray tomograms on the time to find DNA binding sites. *Bull. Math. Biol.* **75**, 2093–2117 https://doi.org/10.1007/s11538-013-9883-9
30 Hagen, C., Guttmann, P., Klupp, B., Werner, S., Rehbein, S., Mettenleiter, T.C. et al. (2012) Correlative Vis-fluorescence and soft X-ray cryo-microscopy/tomography of adherent cells. *J. Struct. Biol.* **177**, 193–201 https://doi.org/10.1016/j.jsb.2011.12.012
31 Duke, E.M.H., Razi, M., Weston, A., Guttmann, P., Werner, S., Henzler, K. et al. (2014) Imaging endosomes and autophagosomes in whole mammalian cells using correlative cryo-fluorescence and cryo-soft X-ray microscopy (cryo-CLXM). *Ultramicroscopy* **143**, 77–87 https://doi.org/10.1016/j.ultramic.2013.10.006
32 Duke, E., Dent, K., Razi, M. and Collinson, L.M. (2014) Biological applications of cryo-soft X-ray tomography. *J. Microsc.* **255**, 65–70 https://doi.org/10.1111/jmi.12139
33 Carzaniga, R., Domart, M.-C., Collinson, L.M. and Duke, E. (2014) Cryo-soft X-ray tomography: a journey into the world of the native-state cell. *Protoplasma* **251**, 449–458 https://doi.org/10.1007/s00709-013-0583-y
34 Hagen, C., Werner, S., Carregal-Romero, S., Malhas A, N., Klupp B, G., Guttmann, P. et al. (2014) Multimodal nanoparticles as alignment and correlation markers in fluorescence/soft X-ray cryo-microscopy/tomography of nucleoplasmic reticulum and apoptosis in mammalian cells. *Ultramicroscopy* **146**, 46–54 https://doi.org/10.1016/j.ultramic.2014.05.009
35 Elgass, K.D., Smith, E.A., LeGros, M.A., Larabell, C.A. and Ryan, M.T. (2015) Analysis of ER-mitochondria contacts using correlative fluorescence microscopy and soft X-ray tomography of mammalian cells. *J. Cell Sci.* **128**, 2795–2804 https://doi.org/10.1242/jcs.169136
36 Conesa, J.J., Otón, J., Chiappi, M., Carazo, J.M., Pereiro, E., Chichón, F.J. et al. (2016) Intracellular nanoparticles mass quantification by near-edge absorption soft X-ray nanotomography. *Sci. Rep.* **6**, 22354 https://doi.org/10.1038/srep22354
37 Chiappi, M., Conesa, J.J., Pereiro, E., Sorzano, C.O.S., Rodríguez, M.J., Henzler, K. et al. (2016) Cryo-soft X-ray tomography as a quantitative three-dimensional tool to model nanoparticle:cell interaction. *J. Nanobiotechnol.* **14**, 15 https://doi.org/10.1186/s12951-016-0170-4
38 Otón, J., Pereiro, E., Pérez-Berná, A.J., Millach, L., Sorzano, C.O.S., Marabini, R. et al. (2016) Characterization of transfer function, resolution and depth of field of a soft X-ray microscope applied to tomography enhancement by Wiener deconvolution. *Biomed. Opt. Express* **7**, 5092–5103 https://doi.org/10.1364/BOE.7.005092
39 Chen, H.-Y., Chiang, D.M.-L., Lin, Z.-J., Hsieh, C.-C., Yin, G.-C., Weng, I.-C. et al. (2016) Nanoimaging granule dynamics and subcellular structures in activated mast cells using soft X-ray tomography. *Sci. Rep.* **6**, 34879 https://doi.org/10.1038/srep34879
40 Varsano, N., Dadosh, T., Kapishnikov, S., Pereiro, E., Shimoni, E., Jin, X. et al. (2016) Development of correlative cryo-soft X-ray tomography and stochastic reconstruction microscopy. A study of cholesterol crystal early formation in cells. *J. Am. Chem. Soc.* **138**, 14931–14940 https://doi.org/10.1021/jacs.6b07584
41 Ramírez-Santiago, G., Robles-Valero, J., Morlino, G., Cruz-Adalia, A., Pérez-Martínez, M., Zaldivar, A. et al. (2016) Clathrin regulates lymphocyte migration by driving actin accumulation at the cellular leading edge. *Eur. J. Immunol.* **46**, 2376–2387 https://doi.org/10.1002/eji.201646291
42 Büchner, T., Drescher, D., Merk, V., Traub, H., Guttmann, P., Werner, S. et al. (2016) Biomolecular environment, quantification, and intracellular interaction of multifunctional magnetic SERS nanoprobes. *Analyst* **141**, 5096–5106 https://doi.org/10.1039/C6AN00890A
43 Schneider, G. (1998) Cryo X-ray microscopy with high spatial resolution in amplitude and phase contrast. *Ultramicroscopy* **75**, 85–104 https://doi.org/10.1016/S0304-3991(98)00054-0
44 Sorrentino, A., Nicolás, J., Valcárcel, R., Chichón, F.J., Rosanes, M., Avila, J. et al. (2015) MISTRAL: a transmission soft X-ray microscopy beamline for cryo nano-tomography of biological samples and magnetic domains imaging. *J. Synchrotron Radiat.* **22**, 1112–1117 https://doi.org/10.1107/S1600577515008632
45 McDermott, G., Le Gros, M.A., Knoechel, C.G., Uchida, M. and Larabell, C.A. (2009) Soft X-ray tomography and cryogenic light microscopy: the cool combination in cellular imaging. *Trends Cell Biol.* **19**, 587–595 https://doi.org/10.1016/j.tcb.2009.08.005
46 Schneider, G., Guttmann, P., Heim, S., Rehbein, S., Mueller, F., Nagashima, K. et al. (2010) Three-dimensional cellular ultrastructure resolved by X-ray microscopy. *Nat. Methods* **7**, 985–987 https://doi.org/10.1038/nmeth.1533
47 Müller, W.G., Heymann, J.B., Nagashima, K., Guttmann, P., Werner, S., Rehbein, S. et al. (2012) Towards an atlas of mammalian cell ultrastructure by cryo soft X-ray tomography. *J. Struct. Biol.* **177**, 179–192 https://doi.org/10.1016/j.jsb.2011.11.025
48 Hagen, C., Dent, K.C., Zeev-Ben-Mordehai, T., Grange, M., Bosse, J.B., Whittle, C. et al. (2015) Structural basis of vesicle formation at the inner nuclear membrane. *Cell* **163**, 1692–1701 https://doi.org/10.1016/j.cell.2015.11.029
49 Hale, V.L., Watermeyer, J.M., Hackett, F., Vizcay-Barrena, G., van Ooij, C., Thomas, J.A. et al. (2017) Parasitophorous vacuole poration precedes its rupture and rapid host erythrocyte cytoskeleton collapse in *Plasmodium falciparum* egress. *Proc. Natl Acad. Sci. U.S.A.* **114**, 3439–3444 https://doi.org/10.1073/pnas.1619441114
50 Ashcroft, J.M., Gu, W., Zhang, T., Hughes, S.M., Hartman, K.B., Hofmann, C. et al. (2008) $TiO_2$ nanoparticles as a soft X-ray molecular probe. *Chem. Commun.* **21**, 2471–2473 https://doi.org/10.1039/b801392f
51 (1896) On a new kind of rays. *Nature* **53** http://www.nature.com/nature/journal/v53/n1369/pdf/053274b0.pdf
52 Sussman, M. (1960) Elementary diffraction theory of zone plates. *Am. J. Phys.* **28**, 394–398 https://doi.org/10.1119/1.1935811
53 Young, M. (1972) Zone plates and their aberrations. *J. Opt. Soc. Am.* **62**, 972–976 https://doi.org/10.1364/JOSA.62.000972
54 Kirz, J., Jacobsen, C. and Howells, M. (1995) Soft X-ray microscopes and their biological applications. *Q. Rev. Biophys.* **28**, 33–130 https://doi.org/10.1017/S0033583500003139
55 Brüggeller, P. and Mayer, E. (1980) Complete vitrification in pure liquid water and dilute aqueous solutions. *Nature* **288**, 569–571 https://doi.org/10.1038/288569a0

© 2018 The Author(s). This is an open access article published by Portland Press Limited on behalf of the Biochemical Society and the Royal Society of Biology and distributed under the Creative Commons Attribution License 4.0 (CC BY).

56 Dubochet, J. and McDowall, A.W. (1981) Vitrification of pure water for electron microscopy. *J. Microsc.* **124**, 3–4 https://doi.org/10.1111/j.1365-2818.1981.tb02483.x
57 Schneider, G., Niemann, B., Guttmann, P., Rudolph, D. and Schmahl, G. (1995) Cryo X-ray microscopy. *Synchrotron Radiat. News* **8**, 19–28 https://doi.org/10.1080/08940889508602810
58 Jacobsen, C. and Kirz, J. (1998) X-ray microscopy with synchrotron radiation. *Nat. Struct. Biol.* **5**, 650–653 https://doi.org/10.1038/1341
59 Maser, J., Jacobsen, C., Kirz, J., Osanna, A., Spector, S., Wang, S. et al. (1998) Development of a cryo scanning transmission X-ray microscope at the NSLS. In *X-ray Microscopy and Spectromicroscopy* (Thieme, J., Schmahl, G., Rudolph, D. and Umbach, E. eds), pp. 35–44, Springer, Berlin, Heidelberg
60 Schneider, G. and Niemann, B. (1998) Cryo X-ray microscopy experiments with the X-ray microscope at BESSY. In *X-ray Microscopy and Spectromicroscopy,* pp. 25–34, Springer, Berlin, Heidelberg
61 Le Gros MA, McDermott, G., Cinquin, B.P., Smith, E.A., Do, M., Chao, W.L. et al. (2014) Biological soft X-ray tomography on beamline 2.1 at the Advanced Light Source. *J. Synchrotron Radiat.* **21**(Pt 6), 1370–1377 https://doi.org/10.1107/S1600577514015033
62 Otón, J., Sorzano, C.O.S., Marabini, R., Pereiro, E. and Carazo, J.M. (2015) Measurement of the modulation transfer function of an X-ray microscope based on multiple Fourier orders analysis of a Siemens star. *Opt. Express* **23**, 9567–9572 https://doi.org/10.1364/OE.23.009567
63 Oton, J., Sorzano, C.O.S., Pereiro, E., Cuenca-Alba, J., Navarro, R., Carazo, J.M. et al. (2012) Image formation in cellular X-ray microscopy. *J. Struct. Biol.* **178**, 29–37 https://doi.org/10.1016/j.jsb.2012.01.006
64 Schneider, G., Guttmann, P., Rehbein, S., Werner, S. and Follath, R. (2012) Cryo X-ray microscope with flat sample geometry for correlative fluorescence and nanoscale tomographic imaging. *J. Struct. Biol.* **177**, 212–223 https://doi.org/10.1016/j.jsb.2011.12.023
65 Smith, E.A., Cinquin, B.P., McDermott, G., Le Gros, M.A., Parkinson, D.Y., Kim, H.T. et al. (2013) Correlative microscopy methods that maximize specimen fidelity and data completeness, and improve molecular localization capabilities. *J. Struct. Biol.* **184**, 12–20 https://doi.org/10.1016/j.jsb.2013.03.006
66 Rehbein, S., Heim, S., Guttmann, P., Werner, S. and Schneider, G. (2009) Ultrahigh-resolution soft-X-ray microscopy with zone plates in high orders of diffraction. *Phys. Rev. Lett.* **103**, 110801 https://doi.org/10.1103/PhysRevLett.103.110801
67 Huang, R. and Bilderback, D.H. (2006) Single-bounce monocapillaries for focusing synchrotron radiation: modeling, measurements and theoretical limits. *J. Synchrotron Radiat.* **13**(Pt 1), 74–84 https://doi.org/10.1107/S0909049505038562
68 Legall, H., Blobel, G., Stiel, H., Sandner, W., Seim, C., Takman, P. et al. (2012) Compact X-ray microscope for the water window based on a high brightness laser plasma source. *Opt. Express* **20**, 18362–18369 https://doi.org/10.1364/OE.20.018362
69 Brooks, R.A. and Di Chiro, G. (1975) Theory of image reconstruction in computed tomography. *Radiology* **117**, 561–572 https://doi.org/10.1148/117.3.561
70 Töpperwien, M., Krenkel, M., Quade, F. and Salditt, T. (2016) Laboratory-based x-ray phase-contrast tomography enables 3D virtual histology. *Proc. SPIE Advances in Laboratory-based X-Ray Sources, Optics, and Applications V*, **9964**, 99640I https://doi.org/10.1117/12.2246460
71 Wolter, H. (1952) Verallgemeinerte Schwarzschildsche Spiegelsysteme streifender Reflexion als Optiken für Röntgenstrahlen. *Ann. Phys.* **445**, 286–295 https://doi.org/10.1002/andp.19524450410
72 Agarwal, K., Sharma, A. and Talukder, G. (1989) Effects of copper on mammalian cell components. *Chem. Biol. Interact.* **69**, 1–16 https://doi.org/10.1016/0009-2797(89)90094-X
73 Mazia, D., Schatten, G. and Sale, W. (1975) Adhesion of cells to surfaces coated with polylysine. Applications to electron microscopy. *J. Cell Biol.* **66**, 198–200 https://doi.org/10.1083/jcb.66.1.198
74 Polisetti, N., Sorokin, L., Okumura, N., Koizumi, N., Kinoshita, S., Kruse, F.E. et al. (2017) Laminin-511 and -521-based matrices for efficient ex vivo-expansion of human limbal epithelial progenitor cells. *Sci. Rep.* **7**, 5152 https://doi.org/10.1038/s41598-017-04916-x
75 Cargill, R.S., Dee, K.C. and Malcolm, S. (1999) An assessment of the strength of NG108-15 cell adhesion to chemically modified surfaces. *Biomaterials* **20**, 2417–2425 https://doi.org/10.1016/S0142-9612(99)00169-6
76 Dobro, M.J, Melanson, L.A, Jensen, G.J. and McDowall, A.W. (2010) Plunge freezing for electron cryomicroscopy. In *Methods in Enzymology* (Jensen, G.J. ed.), pp. 63–82
77 Moor, H. (1987) Theory and practice of high pressure freezing. In *Cryotechniques in Biological Electron Microscopy* (Steinbrecht, R.A. and Zierold, K. ed.), pp. 175–191, Springer, Berlin, Heidelberg
78 Gustafsson, M.G.L., Shao, L., Carlton, P.M., Wang, C.J.R., Golubovskaya, I.N., Cande, W.Z. et al. (2008) Three-dimensional resolution doubling in wide-field fluorescence microscopy by structured illumination. *Biophys. J.* **94**, 4957–4970 https://doi.org/10.1529/biophysj.107.120345
79 Mastronarde, D.N. and Held, S.R. (2017) Automated tilt series alignment and tomographic reconstruction in IMOD. *J. Struct. Biol.* **197**, 102–113 https://doi.org/10.1016/j.jsb.2016.07.011
80 Mastronarde, D.N. (1997) Dual-axis tomography: an approach with alignment methods that preserve resolution. *J. Struct. Biol.* **120**, 343–352 https://doi.org/10.1006/jsbi.1997.3919
81 Kremer, J.R., Mastronarde, D.N. and McIntosh, J.R. (1996) Computer visualization of three-dimensional image data using IMOD. *J. Struct. Biol.* **116**, 71–76 https://doi.org/10.1006/jsbi.1996.0013
82 Radermacher, M. (2007) Weighted back-projection methods. In *Electron Tomography* (Frank, J. ed.), pp. 245–273, Springer, New York
83 Wolf, D., Lubk, A. and Lichte, H. (2014) Weighted simultaneous iterative reconstruction technique for single-axis tomography. *Ultramicroscopy* **136**, 15–25 https://doi.org/10.1016/j.ultramic.2013.07.016
84 (2017) SOLUTION — Amira for Life Sciences. https://www.fei.com/software/amira-for-life-sciences/
85 Haubold, C., Schiegg, M., Kreshuk, A., Berg, S., Koethe, U. and Hamprecht, F.A. (2016) Segmenting and tracking multiple dividing targets using ilastik. *Adv. Anat. Embryol. Cell Biol.* **219**, 199–229 https://doi.org/10.1007/978-3-319-28549-8_8
86 Chen, M., Dai, W., Sun, S.Y., Jonasch, D., He, C.Y., Schmid, M.F. et al. (2017) Convolutional neural networks for automated annotation of cellular cryo-electron tomograms. *Nat. Methods* **14**, 983–985 https://doi.org/10.1038/nmeth.4405
87 Arganda-Carreras, I., Kaynig, V., Rueden, C., Eliceiri, K.W., Schindelin, J., Cardona, A. et al. (2017) Trainable Weka Segmentation: a machine learning tool for microscopy pixel classification. *Bioinformatics* **33**, 2424–2426 https://doi.org/10.1093/bioinformatics/btx180
88 Hecksel, C.W., Darrow, M.C., Dai, W., Galaz-Montoya, J.G., Chin, J.A., Mitchell, P.G. et al. (2016) Quantifying variability of manual annotation in cryo-electron tomograms. *Microsc. Microanal.* **22**, 487–496 https://doi.org/10.1017/S1431927616000799
89 Darrow, M.C., Luengo, I., Basham, M., Spink, M.C., Irvine, S., French, A.P. et al. (2017) Volume segmentation and analysis of biological materials using SuRVoS (Super-region Volume Segmentation) Workbench. *J. Vis. Exp.* **126** https://doi.org/10.3791/56162



© 2018 The Author(s). This is an open access article published by Portland Press Limited on behalf of the Biochemical Society and the Royal Society of Biology and distributed under the Creative Commons Attribution License 4.0 (CC BY).